High Quality Carbon Nanotubes on Conductive Substrates Grown at Low Temperatures

*Muhammad Ahmad, Jose V. Anguita, Vlad Stolojan, Tony Corless, Jeng-Shiung Chen, J. David Carey, and S. Ravi P. Silva**

For carbon nanotubes (CNTs) to be exploited in electronic applications, the growth of high quality material on conductive substrates at low temperatures (<450 °C) is required. CNT quality is known to be strongly degraded when growth is conducted on metallic surfaces, particularly at low temperatures using conventional chemical vapor deposition (CVD). Here, the production of high quality vertically-aligned CNTs at low substrate temperatures (350–440 °C) on conductive TiN thin film using photo-thermal CVD is demonstrated by confining the energy required for growth to just the catalyst using an array of optical lamps and by optimizing the thickness of the TiN under-layer. The thickness of the TiN plays a crucial role in determining various properties including diameter, material quality, number of shells, and metallicity. The highest structural quality with a visible Raman D- to G-band intensity ratio as low as 0.13 is achieved for 100 nm TiN thickness grown at 420 °C; a record low value for low temperature CVD grown CNTs. Electrical measurements of high density CNT arrays show the resistivity to be 1.25×10^{-2} Ω cm representing some of the lowest values reported. Finally, broader aspects of using this approach as a scalable technology for carbon nanomaterial production are also discussed.

1. Introduction

High structural quality and low temperature chemical vapor deposition (CVD) of carbon nanotubes (CNTs) on conducting surfaces is essential in order to utilize their attractive electronic properties for a number of applications such as CNT-based electronic devices, sensors, field emission, through-Si-vias, and CMOS interconnects.[1–6] The quality of CNTs produced can be judged by various methods such as TEM imaging, electrical characterization, visible Raman I_D/I_G ratio analysis, etc. Amongst others, the Raman I_D/I_G ratio analysis method is the most common for judging both electronic and structural quality of CNTs; lower I_D/I_G values indicate better CNT quality.[7] CNTs produced by arc-discharge or laser ablation-based methods typically show the highest material quality, though such production methods are incompatible with microelectronics and complementary metal oxide semiconductor (CMOS) technologies due to the prohibitively high growth temperatures (3000–4000 °C) present.[5] Furthermore, in-situ patterned growth of vertically aligned CNTs, which is a requirement in many electrical and electronic applications, is not possible using either of these methods. Considerable progress has been made to improve the yield and quality of CVD grown CNTs on insulating surfaces, such as SiO_2 or alumina,[8–10] however similar progress has been lacking in the growth of CNTs on metallic surfaces. The general approach to achieve high quality CNTs, regardless of the substrate type, is to use elevated growth temperatures in the range of 600–1100 °C,[7,11–13] which cannot be applied where temperature sensitive substrates are used or tight thermal budgets are present. Shamsudin et al.[11] produced CNTs in their two stage CVD system using camphor oil (carbon feedstock) and ferrocene (catalyst) in the temperature range of 700–900 °C and found the corresponding Raman I_D/I_G ratio decreased from 0.72 to 0.52. Meshot et al.[14] in their decoupled CVD method used a substrate temperature from 675–875 °C for the growth of CNTs on Si/SiO_2 samples coated with Al_2O_3/Fe and found the I_D/I_G ratio decreased from 1.3 to 0.5. Kim et al.[13] performed CVD growth of CNTs on silicon dioxide substrate using acetylene (carbon feedstock) and ferrocene (catalyst), in the temperature range of 600–800 °C and reported a corresponding decrease in I_D/I_G ratio from 0.87 to 0.44. Lee et al.[15] conducted CNT growth in the temperature range of 800–1100 °C using C_2H_2 (carbon feedstock) and Fe particles (catalyst) coated on Si substrate and found I_D/I_G ratio decreased from 0.82 to 0.45. Although, CNT growth at low temperatures (400–500 °C) on metallic surfaces has been demonstrated by a number of groups,[16–21] the quality of CNTs is largely degraded when the growth is conducted at low temperatures.[7] As a consequence

Dr. M. Ahmad, Dr. J. V. Anguita, Dr. V. Stolojan, T. Corless, Dr. J.-S. Chen, Dr. J. D. Carey, Prof. S. R. P. Silva
Advanced Technology Institute
University of Surrey
Guildford GU2 7XH, UK
E-mail: s.silva@surrey.ac.uk
Dr. J. D. Carey, Prof. S. R. P. Silva
Department of Electronic Engineering
University of Surrey
Guildford GU2 7XH, UK

DOI: 10.1002/adfm.201501214

the realization of high quality CNT growth at low temperatures on conductive substrates has proven to be challenging. Here, we demonstrate high quality (I_D/I_G: 0.97–0.13) nanotube growth at low substrate temperatures, 350–420 °C, on conductive TiN layer using photothermal chemical vapor deposition (PTCVD).

PTCVD is a potentially large scale production method that relies on high power optical sources to deliver energy onto the growth surface while the bulk of the substrate is held at much lower temperatures.[22–24] We show that high quality growth of CNTs is achieved through engineering the thickness of the underlying TiN layer such that the energy necessary for growth is concentrated into the metallic catalyst with little being transmitted to the underlying substrate. The tuning of the TiN thickness results in a controllable catalyst diameter accompanied by a narrow spread in diameter distribution; correct engineering of the TiN thickness to concentrate optical energy is therefore crucial for the production of high quality CNTs with controlled diameter. This method of concentrating optical energy at the catalyst or growth front by optimizing the thickness of an under layer has not been previously reported and provides a route to achieve scalable production of high quality nanomaterials with tunable properties at low temperature. Electrical characterization of CNT-based vias fabricated in a chain structure is also performed, where the vias are connected by alternating top and bottom metal lines. The resistance values measured for two sizes of vias, 10×10 and 5×5 μm^2, are 25 and 100 Ω, respectively, representing some of the lowest resistance for CNT-based vias when compared with recent studies.[20,25–28]

2. Results and Discussion

2.1. CNT Growth on Metallic TiN–Si Substrates

CNT growth is carried out on *n*-Si substrate coated with TiN, Al (10 nm) and Fe (3 nm), respectively (**Figure 1**a), using a PTCVD system Figure 1b. The thickness of the TiN film is varied from 50 to 200 nm on various samples. Electron microscopy images (45° tilted) of CNTs grown in a bulk substrate temperature range of 350–440 °C (corresponding catalyst surface temperature is 550–715 °C) for various thicknesses of TiN layers are shown in **Figure 2**. The images of the CNTs grown at 375 and 420 °C are given in the Figure S1 of the Supporting Information. It can be observed that the growth of CNTs is not only sensitive to the temperature but also to the thickness of the TiN under layer. For example, vertically aligned CNT growth is achieved for 50 and 100 nm TiN films at 350 °C, whereas short and tangled CNT growth is achieved for 150 and 200 nm TiN films. Furthermore, the nanotube density grown at 400°C is estimated to be 2×10^{10} and 8×10^{10} cm^{-2} for 50 nm TiN and 100 nm TiN films, respectively, using the weight gain method described by Esconjauregui et al.[29] (detail given in the Supporting Information). The CNT growth profile for the two parameters, temperature and the thickness of the TiN layer, is summarized in **Table 1**.

Visible Raman spectra, using 514 nm laser excitation wavelength, of the as-grown CNTs are presented in **Figure 3**. Well-defined first and second order Raman features are observed with a D peak centered at 1340 cm^{-1}, a G peak around 1580 cm^{-1} and a 2D peak around 2680 cm^{-1}. The normally Raman inactive D peak becomes active in presence of defects with its intensity increasing with defect concentration or in the presence of amorphous carbon.[30] The strongest feature in the Raman spectra is the G peak associated with the Raman-active E_{2g} vibration of sp^2 bonded carbon atoms and its presence is a signature of graphitization in the material. The intensity of the G peak increases as the degree of graphitization in the material increases, therefore, the intensity ratio of the D peak to the G peak (I_D/I_G) is often used as a quantitative measure of material quality of a graphite-like materials.[31] The 2D peak is the overtone of the D peak but its intensity does not increase with defects, since in this second order Raman process both scattering events are phonon assisted.[30] The intensity of the 2D peak is reported to increase as the quality of the material increases.[30,32,33]

We find the I_D/I_G ratio of as-grown CNTs varies from 0.97 to 0.13 over the entire growth temperature range of 350–440 °C. Lower I_D/I_G values and higher intensity 2D peaks are indicative of higher quality of CNTs. Behler et al.[34] performed vacuum heat treatment (up to 2000 °C) to grow CVD MWCNTs and found higher intensity of the 2D peak in the Raman spectra of heat-treated CNTs and a decrease in the I_D/I_G ratios as the material became more graphitic, which is also supported by their TEM analysis. For comparison, the general trend of I_D/I_G ratios (for 514 nm laser wavelength) reported in the literature[7,11–13] is found to decrease from 0.9 to 0.4 as the CNT growth temperature is increased from 600 to 1100 °C. The I_D/I_G ratio is much higher (>2) for CNTs grown in the low temperature range

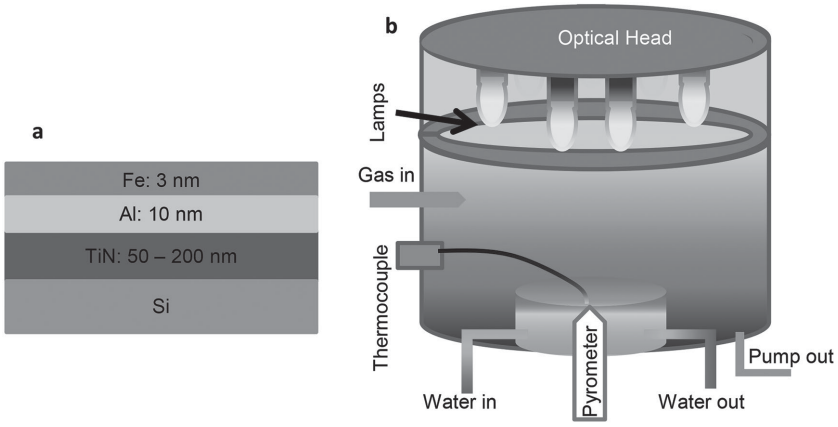

Figure 1. a) Schematic of the layer structure. The thickness of the TiN is varied from 50 to 200 nm while the Al (10 nm) and Fe (3 nm) layer thickness is kept constant for all samples. b) Schematic of photothermal CVD (PTCVD). Optical energy is delivered from the top while the sample is placed on a water-cooled chuck. The bulk temperature of the substrate is measured by a pyrometer at the bottom side whereas the catalyst surface temperature is measured by a thermocouple.

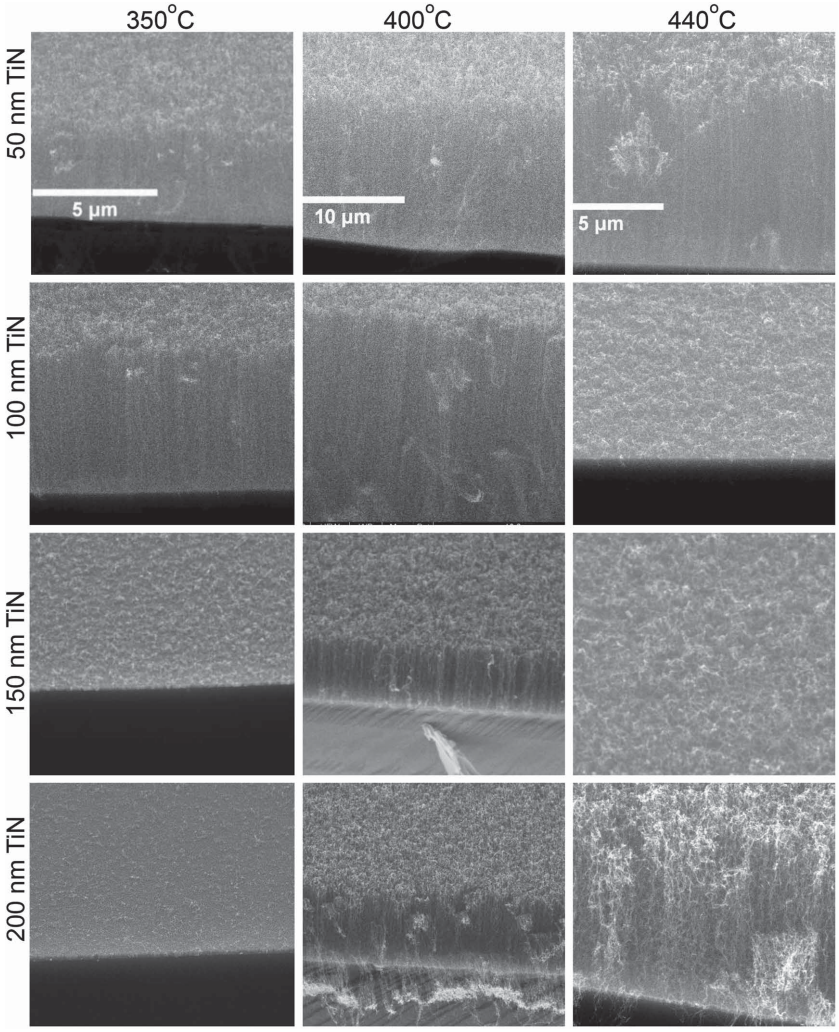

Figure 2. Scanning electron microscopy images (45° tilted) of the CNTs grown at substrate temperatures 350, 400, and 440 °C for different thicknesses of TiN from 50 to 200 nm as indicated in each row. The scale bar for all the images in each column is the same.

(400–550 °C).[7,35] Thus, the overall low I_D/I_G ratios and the presence of well-developed 2D peaks in the Raman spectra of Figure 3 are indicative of high quality nanotubes grown in the low temperature range.

The key observation in Figure 3 is the change in the I_D/I_G values at a constant temperature when the TiN thickness is changed. For example, the CNTs grown at 400 °C the I_D/I_G values are 0.65, 0.25, 0.24, and 0.63 for 50, 100, 150, and 200 nm TiN, respectively. This result shows that the quality of the CNTs has been largely decoupled from the temperature of the substrate and now depends strongly on the TiN thickness. This de-coupling between growth and substrate parameters is an important result of the approach presented here. Previously, improving the CNT quality necessitated a rise in the growth temperature, thereby posing a hindrance for growth on temperature-sensitive substrates. The Raman spectrum of the CNTs grown at 420 °C for the 100 nm TiN (Figure 3) shows a small D peak, I_D/I_G ratio of 0.13 ($I_G/I_D \approx 8$), which is a record low value when compared with other low temperature grown CNTs on conductive substrates using conventional CVD methods[7,35] and comparable in quality to the arc-discharge produced CNTs.[36]

In **Figure 4**a–c, the I_D/I_G ratio, FWHM (full width at half-maximum) of the G peak and growth rate of the as-grown CNTs are plotted as a function of the TiN thickness over the entire temperature range (350–440 °C). The dependence of I_D/I_G values on both temperature and thickness of the TiN layer can be observed in Figure 4a. While the decrease in the I_D/I_G values with increasing growth temperature is in-line with previous studies,[11–13] the dependence on the thickness of conductive TiN under layer has not been revealed previously and therefore acts as an independent growth control parameter. The dependence of the I_D/I_G on TiN thickness is found to be more sensitive at higher temperatures (400–440 °C) than at lower temperatures (350–375 °C). In Figure 4b, the values of the FWHM of the G peak range from 90 to 29 cm^{-1} and the trend of the FWHM as a function of the TiN thickness for 350–440 °C is observed to be similar to that of I_D/I_G shown in Figure 4a. The lower values of I_D/I_G and sharper G peak is related to the higher structural quality of CNTs.[37] Thus, a Raman G peak FWHM of 29 cm^{-1} and a corresponding

Table 1. Growth profile of as-grown CNTs at various temperatures on the samples containing the thickness of TiN from 50 to 200 nm. VCNT = vertically aligned carbon nanotubes.

TiN thickness [nm]	Growth temperature				
	350 °C	375 °C	400 °C	420 °C	440 °C
50	VCNTs	VCNTs	VCNTs	VCNTs	VCNTs
100	VCNTs	VCNTs	VCNTs	Short VCNTs	Short tangled
150	Short tangled	VCNTs	VCNTs	Short VCNTs	Tangled
200	Short tangled	Short VCNTs	VCNTs	Tangled	VCNTs

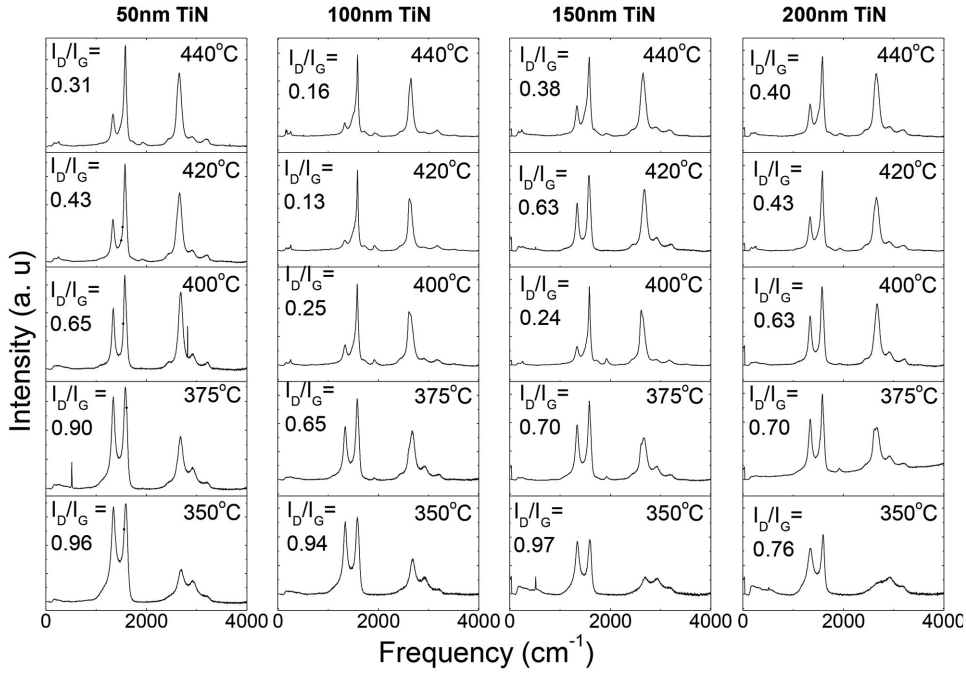

Figure 3. Visible Raman spectra of the CNTs grown as a function of temperature and thickness of the TiN layer. The spectra show well-defined Raman features; a G peak around 1582 cm^{-1}, a D peak around 1338 cm^{-1}, and a 2D peak around 2660 cm^{-1}. The I_D/I_G ratios show strong dependence on the growth temperature, as well as on the thickness of the TiN layer.

I_D/I_G ratio of 0.13 represents high quality CNTs grown at 420 °C on 100 nm TiN thickness.

In Figure 4c, the growth rate of CNTs at different temperatures is plotted as a function of the thickness of TiN layer. Over the entire temperature range, the growth rate ranges from 0.9–5, 0.7–5.6, 0.4–1.4, and 0.3–2 µm min^{-1} for 50, 100, 150, and 200 nm thicknesses of the TiN layer, respectively. The overall trend of the growth rate is first to increase and then decrease with increasing temperature, which is attributed to the poisoning of the catalyst at higher temperatures.[38] The highest

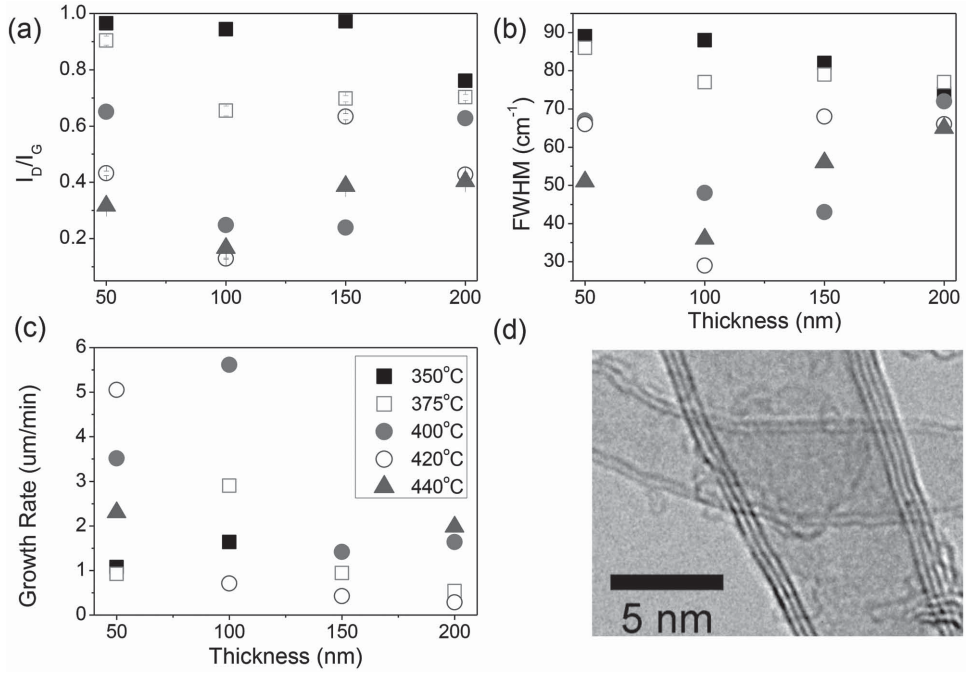

Figure 4. a–c) Variation of the Raman I_D/I_G ratio, FWHM of the Raman G peaks and nanotube growth rate verses thickness of the TiN layer for various temperatures. d) Representative transmission electron microscopy image of the CNTs grown at 400 °C for 100 nm TiN.

achieved growth rate is 5.6 μm min^{-1} for CNTs grown at 400 °C on the sample containing a 100 nm thick TiN underlayer, which is a significantly higher value than reported in literature, typically 0.05–1.3 μm min^{-1} for CNTs grown on metallic layers at low temperatures.[20,25,39] Figure 4d shows a representative TEM image of CNTs grown at 400 °C on a 100 nm thick TiN layer and reveals that the nanotubes are clean, maintain a long range structural order and free of amorphous carbon. Statistical analysis of over 100 nanotubes reveals that there are MWCNTs with 9 ± 3 nm diameter and 4 ± 2 shells for 50 nm TiN thickness, whereas the CNTs for 100 nm TiN are mainly double-walled (2 ± 1 shells) with a diameter of 5 ± 1 nm, but a considerable fraction of single-walled and triple-walled CNTs are also observed. Similar analysis can also be performed using UHV STM studies.[40]

The production yield of semiconducting and metallic SWCNTs can be estimated by analyzing the RBM (radial breathing mode) region of the Raman spectra.[24,41] With a laser energy of 2.41 eV (514 nm wavelength), 150 to 210 cm^{-1} spectral range corresponds to semiconducting SWCNTs whereas 210 to 280 cm^{-1} corresponds to metallic SWCNTs.[41] The CNTs grown from the 100 and 150 nm TiN at 400, 420, and 440 °C contain a considerable fraction of SWCNTs, a representative TEM image showing SWCNTs is given in Figure S2 of the Supporting Information, which allows us to analyze their Raman spectra in order to estimate the respective type of as-grown SWCNTs. **Figure 5**a–c show the RBM spectra of the CNTs grown from 100 nm TiN; the spectra are normalized with respect to the G-band intensity and analyzed by the Lorentz function. It can be observed that at 420 °C (Figure 5b) and 400 °C (Figure 5c), there is a preferential growth of metallic SWCNTs and as the temperature increases to 440 °C, the sample is dominated by the semiconducting SWCNTs (Figure 5c). In order to compare the preferential growth quantitatively,[24] the ratio of the total intensity of the Raman spectra from the RBMs to the G-band intensity, I_{RBM}/I_G, of the samples grown from 100 and 150 nm TiN from 400 to 440 °C is shown in Figure 5d. It can be observed that the production yield of SWCNT is enhanced with increasing the growth temperature and the CNTs grown from 100 nm TiN possess higher yield of SWCNTs as compared with the CNTs grown from 150 nm TiN. Furthermore, the sample grown from the 100 nm TiN at 420 °C exhibits the highest preferential growth of metallic SWCNTs.

The key result from Figures 4 and 5 is the highest quality and preferential growth of metallic CNTs, as judged by Raman spectra analysis, is found at 100 nm TiN layer thickness. In order to understand this result, **Figure 6**a–d shows atomic force microscope images of the Fe catalyst islands formed on samples of 50, 100, 150, and 200 nm TiN annealed at 400 °C for 10 min in H_2 environment at 2 Torr pressure. A Gaussian fit to the measured particle diameter distribution is shown in Figure 6e, where the mean diameter of the catalyst particles is found to be 10 ± 6, 5 ± 3, 7 ± 5, and 7 ± 4 nm for 50, 100, 150, and 200 nm TiN thick layers, respectively. The mean particle diameter of 10 ± 6 nm and 5 ± 3 nm for 50 nm and 100 nm TiN layers resulted in the CNTs of the mean diameter of 9 ± 3 and 5 ± 1 nm, respectively, as found via TEM analysis. In Figure 6f–h, the mean catalyst diameter, standard deviation and

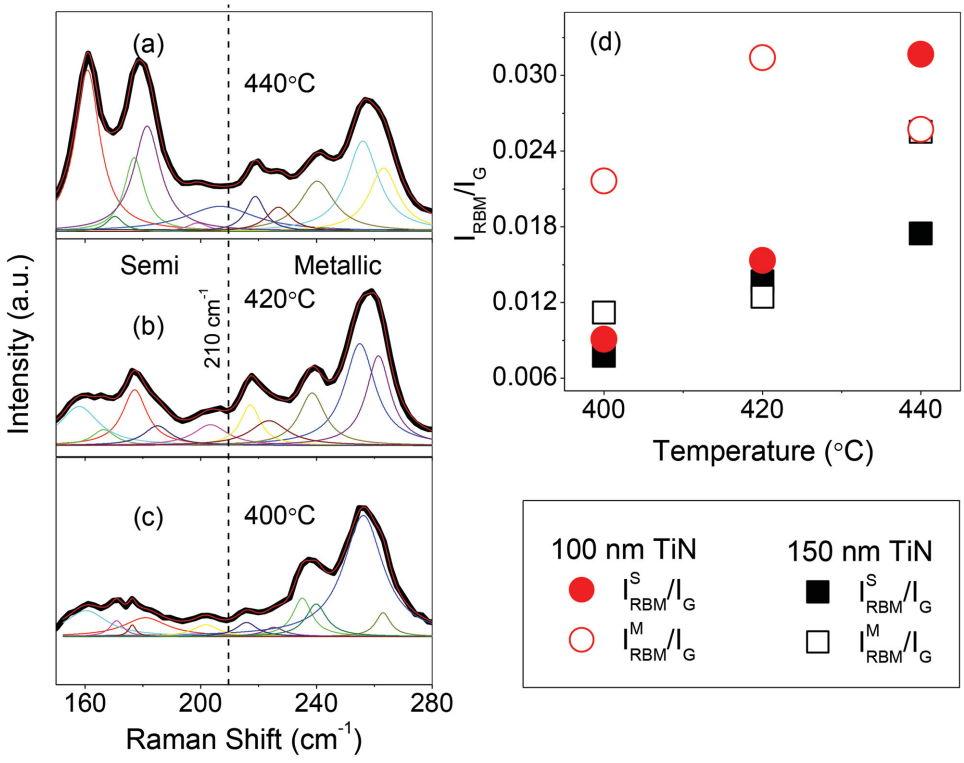

Figure 5. a–c) Raman radial breathing (RBM) mode spectra of the CNTs grown from 100 nm TiN. d) The variation of the intensity ratio of the summed RBM intensity to the G-band intensity to the growth temperature. Here I^S_{RBM}/I_G and I^M_{RBM}/I_G represent the RBM intensity ratio of semiconducting and metallic tubes to the G band intensity, respectively.

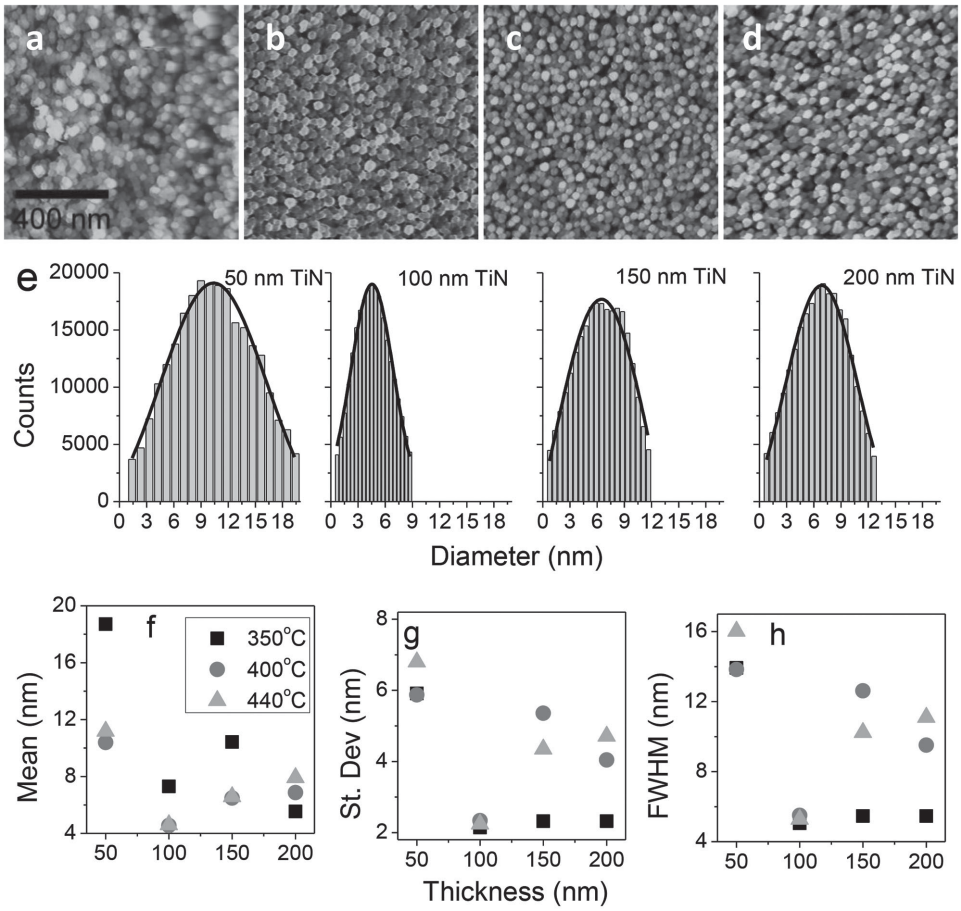

Figure 6. a–d) Atomic force microscope images of the samples annealed for 10 minutes at 2 Torr H_2 pressure at 400 °C, containing 50, 100, 150, and 200 nm TiN layers, respectively. The scale bar given in (a) is also valid for (b–d). e) The Gaussian fitted diameter distribution of the Fe catalyst nanoparticles for the respective thickness of the TiN layer. f–h) Mean diameter, standard deviation, and FWHM of Gaussian curves are plotted as a function of the TiN thickness for 350, 400, and 440 °C temperatures, respectively.

FWHM determined by Gaussian fit are plotted as a function of the thickness of TiN layer for 350, 400, and 440 °C annealing temperatures, which also show a dependence on the thickness of the TiN layer. In each case the minimum value measured is found to occur at a thickness of 100 nm TiN.

From Figures 4–6, the thickness of the TiN layer plays a crucial role in determining both catalyst morphology and subsequent nanotube properties. Key to PTCVD is the ability to engineer the substrate parameters to reflect the optical energy to the topmost layer, that is, the catalyst. We calculate the wavelengths for thin film constructive interference, and hence maximum energy reflected to the catalyst is at 240, 480, 720, and 960 nm for 50, 100, 150, and 200 nm layer thicknesses of TiN, respectively. The reflectance of the structure of Figure 1a has been calculated[42] and is shown in **Figure 7**. Wavelengths below 300 nm are blocked by the quartz plate in front of the lamps and hence are not present in the chamber during the growth. Analysis of Figure 7 shows that the energy reflected back to the catalyst by the TiN–Si interface can be controlled effectively by adjusting the thickness of the TiN layer. This enables us to engineer the condition for maximum coupling of energy at the CNT growth front which results in the growth of extremely high quality CNTs, despite growth at a low substrate temperature (420 °C). For example, for the samples with 50 nm TiN layer (solid line in Figure 7a), little energy is reflected to the catalyst, whereas for 100 nm TiN layer (dashed line), a single broad peak of reflected light centered around 480 nm supplies continuously high energy at the growth front of CNTs, hence the lowest I_D/I_G (highest material quality) values are achieved at all temperatures compared with all of the other selected thicknesses of TiN. For the samples containing 150 and 200 nm TiN, an alternating pattern of constructive and destructive peaks is observed (Figure 7b), resulting in lower coupling of energy reflected back to the catalyst layers and lower growth rates. The method of concentrating optical energy at the growth front by tuning the thickness of underlying layer for the growth of high quality material at low temperatures may not be limited to the CNT growth; it can be readily extended for PTCVD growth of other materials, such as graphene.

2.2. Electrical Characterization of CNT Based Vias

High density forests of high quality CNTs grown at low temperatures can be employed for a wide range of CNT-based electronic devices, field emission display, through-Si-vias (TSV)

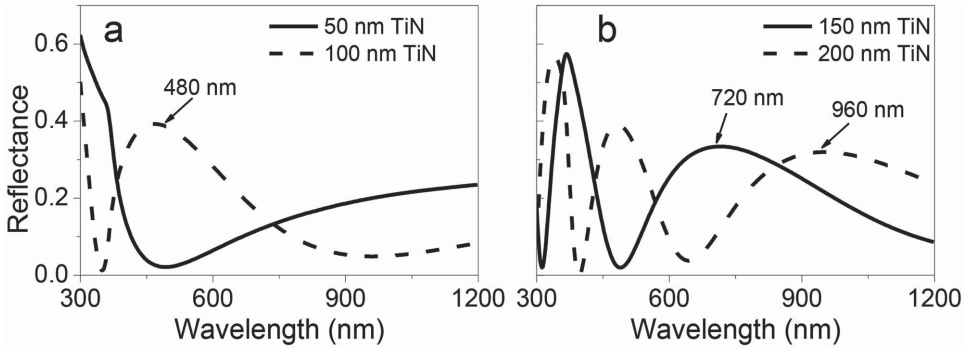

Figure 7. Simulated reflectance of the Si/TiN structure as a function of wavelength for a) 50 nm and 100 nm TiN thicknesses and b) for 150 and 200 nm TiN thicknesses, respectively.

and interconnect applications. For all these applications, high electrical conductivity of CNT bundles is needed. In order to measure the conductivity of the CNTs, vias are fabricated using the process flow outlined in **Figure 8**. The CNT-based vias are fabricated in a chain structure where each via is connected by the alternating top (M2) and bottom metal (M1: Ti/Cu/TiN) lines. Two different sizes of vias, 10×10 and 5×5 μm^2, are fabricated to distinguish the resistance of vias from the metal lines. The center-to-center distance of neighboring vias is set to 50 μm and the dimensions of the metal lines for both M1 and M2 are set to 65 μm (length) and 15 μm (width). The number of vias in a chain structure is varied from 2 to 100 for both 10×10 and 5×5 μm^2 sizes.

Scanning electron microscopy images of the CNT-based vias are shown in **Figure 9**. A uniform vertically aligned CNT growth occurred in all holes, producing a 100% yield. The length of the as-grown CNTs is 20 ± 3 μm and from electron microscopy analysis the estimated nanotube density is 10^{10} cm^{-2}. Figure 9a is a tilted (45°) scanning electron microscope (SEM) image of 100 CNT-based vias of 10×10 μm^2 area and Figure 9b,c are corresponding magnified images. Figure 9d,e are the images for 5×5 μm^2 CNT-based vias. Figure 9f is a representative TEM image showing clean (i.e., no catalyst particles present or amorphous carbon layer), hollow and well graphitized multiwall CNT (MWCNT) maintaining a long-range crystalline order. Analysis of over 150 nanotubes shows that their average diameter is 14 ± 4 nm and average number of shells is 9 ± 4. The Raman I_D/I_G ratio is 0.5 for these nanotubes, comparable to the CNTs grown above 800 °C using conventional CVD techniques.[12] It is worth noting that the profile of CNTs grown on Ti/Cu/TiN layer structure (in vias) is different than the CNTs grown on 50 nm TiN under layer (Figure 2) at the same temperature (400 °C), indicating the effect of additional under layers (Ti/Cu) on the growth of CNTs. For example, the value of I_D/I_G, average diameter and average number of shells per CNT for growth on a 50 nm TiN underlayer is 0.62, 9 nm and 4 respectively, whereas these values are 0.5, 14 nm and 9 for the CNTs grown over Ti/Cu/TiN layer structure.

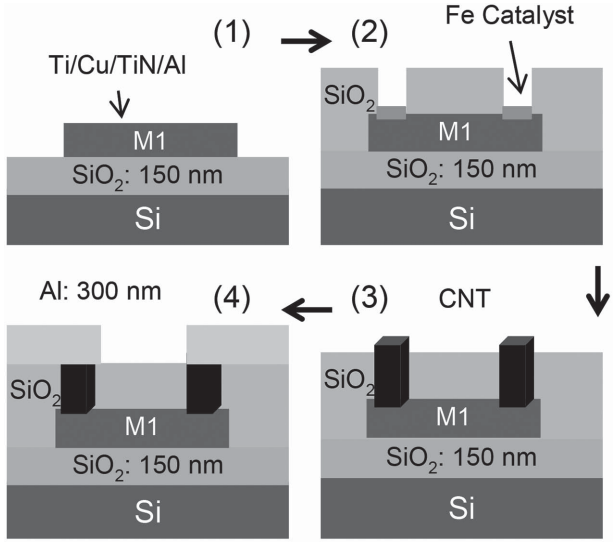

Figure 8. Process flow for the fabrication of CNT-based vias. A layer stack of Ti/Cu/TiN (50/200/50 nm) is sputter deposited on a 150 nm SiO_2 coated Si substrate and patterned lithographically using lift-off process (step 1). After this a 300 nm SiO_2 film is grown and patterned to define via holes (step 2). A layer stack of Al/Fe (10/3 nm) is sputter deposited as catalyst for CNT growth. CNT growth is conducted in a PTCVD system and a 300 nm Al film (M2) is sputter deposited and patterned to form top contact.

Figure 9g shows the lower magnified SEM image of a completed via chain structure after patterning with 300 nm Al (M2) as a top metal contact. No filler material is deposited to hold the CNTs in vias and no chemical mechanical polishing (CMP) has been applied. Al is directly deposited onto as-grown CNTs, and then patterned and etched. In this way, CNT contact with solvents, which is inevitable if a lift-off process is used which often leads to deformation of their alignment through densification,[43] can be avoided. Figure 9h shows a 300 nm Al coated CNT via where the formation of uniform top metal-CNT contact can be observed. It is important to note that the electrical conduction in the vias is expected through the whole length of CNTs, from top to the root, since: (1) most of the CNTs are in contact with the metal (Al) at the top and (2) conduction in a CNT bundle is anisotropic.[44] Indeed, the outermost CNTs in the ring of the square vias are in contact with the metal from the sides and may conduct from there. However, Vo et al.[44] showed that the contribution of these CNTs in the total conduction would be negligible because of the small number of tubes present at the outermost ring.

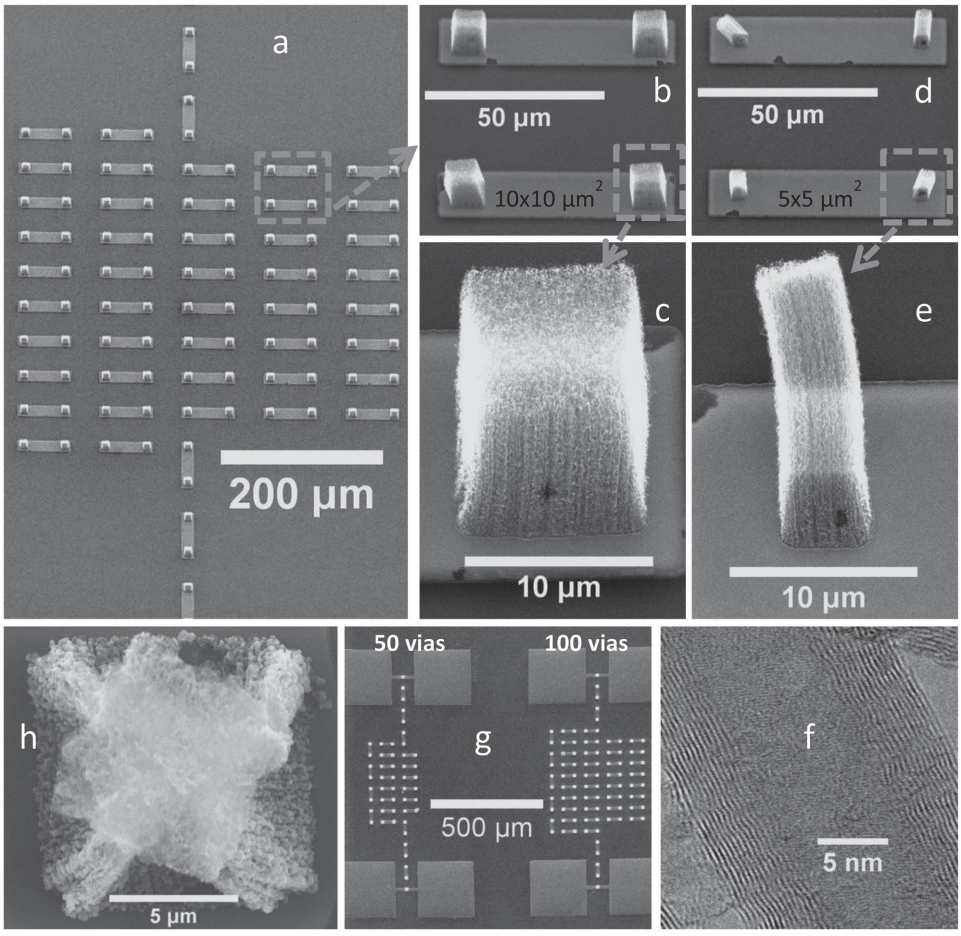

Figure 9. a) Scanning electron microscopy image of PTCVD grown CNTs in 100 vias of 10×10 µm^2 size on bottom metal strips (M1). b–e) Magnified images for the CNTs grown in vias of 10×10 and 5×5 µm^2 sizes on M1. f) High resolution transmission electron microscope image shows straight and well graphitized walls of in multiwall CNTs. g) Structures containing 100 and 50 vias after the deposition of 300 nm Al as a top metal contact (M2). h) Magnified image of CNT-based via after deposition of 300 nm Al as top metal (M2).

There are different views on whether to use MWCNTs or single-wall CNTs (SWCNTs) for enhanced electrical conductivity and applications.[45–47] The performance analysis of Li et al.[45] of SWCNTs being better than MWCNTs is mainly because of their calculations of lower density of conducting CNT shells when MWCNTs are used. This happens because of the assumptions that all SWCNTs are metallic and the inner diameter of a MWCNT is half of its outer diameter, which in our view is an underestimate for a MWCNT. About a third of SWCNTs in a bundle are expected to be metallic, however for MWCNTs even semiconducting shells are expected to become effectively metallic because of their larger diameter, as is mentioned in the same study.[45] Majumder et al.[46] presented their analysis showing better performance of MWCNTs over SWCNTs in terms of cross-talk based induced time delay in the metal lines. A single MWCNT can be used in a via hole of up to 60 nm diameter instead of using a bundle of SWCNTs which may provide ease and reliability in the process.[48] Growth of MWCNTs is relatively easy and cost effective as compared with that of SWCNTs. Electrical conduction through the contribution of subbands in MWCNTs has been observed[40] and a conductance of $460G_0$ has been reported for a MWCNT having 74 shells, which exceeds the maximum expected value of $148G_0$.[49] A negative thermal coefficient of resistance for MWCNT-based vias has also been reported which is particularly suitable for interconnect applications where the operating temperature is generally above 90 °C.[20]

In **Figure 10**a, current–voltage characteristics of the structures containing 100 vias of both 10×10 and 5×5 µm^2 sizes, before and after thermal annealing, are presented. A significant improvement in the conductivity is achieved after annealing the sample, which is the result of improved metal-CNT contacts. Figure 10b shows that the resistance of the structures increases linearly as the number of vias increase. The measured resistance of the chain structure is the sum of the total resistance of the CNT-based vias and that of the metal lines. The mean (and standard error) resistance of a single via and a single metal line, before annealing, for the structures containing 10×10 and 5×5 µm^2 vias is

$$R_{T10} = R_{v10} + R_m = 785 \pm 51\ \Omega \quad (1)$$

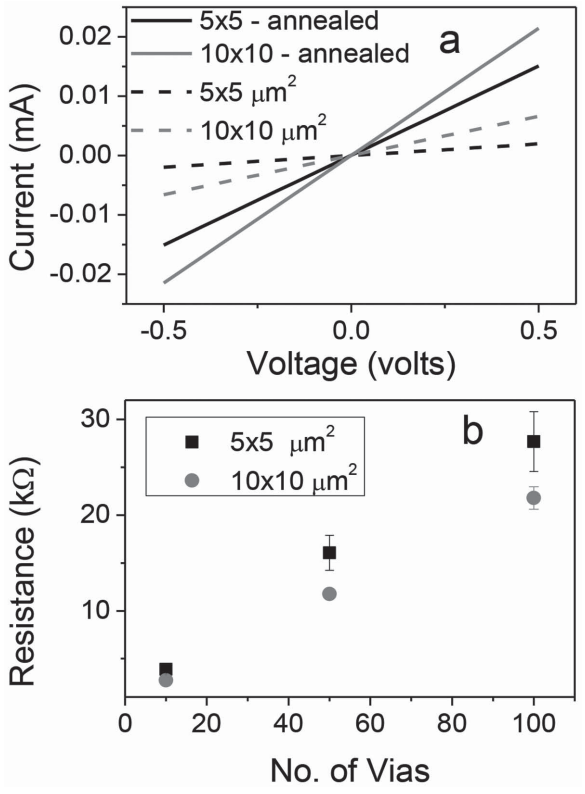

Figure 10. a) Current–voltage characteristics of 100 CNT-based vias for both structures containing 10 × 10 and 5 × 5 μm² vias, before and after annealing. The linear current–voltage relationship indicates a good Ohmic contact. b) Electrical resistance as a function of number of vias.

and

$$R_{T5} = R_{v5} + R_m = 2448 \pm 267\Omega \quad (2)$$

where R_{T10} and R_{T5} are the total resistances of the structures containing 10 × 10 μm² vias and 5 × 5 μm² vias, respectively, R_{v10} and R_{v5} are the resistances of a single 10 × 10 and a 5 × 5 μm² CNT-based vias, respectively and R_m is the resistance of a metal line. Since the dimensions, and hence resistance, of the metal lines are the same for both sizes of vias, subtracting Equation (1) from Equation (2) gives

$$R_{T5} - R_{T10} = R_{v5} - R_{v10} = 1663 \pm 272\Omega \quad (3)$$

As the resistance of a CNT bundle is inversely proportional to the number of conducting tubes, R_{v5} is taken as four times larger than R_{v10}, since 5 × 5 μm² via would have 1/4 the number of tubes (2500 tubes) as that of 10 × 10 μm² via (10^4 tubes), assuming a CNT density of 10^{10} per cm². Using this relationship, R_{v5} and R_{v10} are calculated from Equation (3) as 2217 ± 363 and 554 ± 91 Ω, respectively. After annealing, the values for R_{T5} and R_{T10} are found to be 351 ± 20 and 276 ± 18 Ω; the corresponding values for R_{v5} and R_{v10} are 100 ± 36 and 25 ± 9 Ω, respectively.

The resistance values after annealing the samples are reduced significantly, and are attributed to the improved electrical contact between the metal and CNTs. The reduction in resistance with annealing has been previously reported[28,50,51] though not to such low values as that found here. Katagiri et al.[50] noted a decrease in the resistance from 3.8 to 1.5 kΩ after annealing of a 160 nm diameter CNT-based via and Chiodarelli et al.[28] reported a decrease from 26 to 7.9 kΩ (from 104 to 40 Ω for 576 vias in parallel) of 300 nm diameter CNT-based via. Our resistance values, corresponding to a resistivity of 1.25×10^{-2} Ω cm, are lower when compared with the CNT-based vias reported in the literature.[20,25,26,44] For example, upon scaling to the equivalent dimensions the values of the 5 × 5 and 10 × 10 μm² vias reported by Dijon et al.[26] (resistivity = 7.85×10^{-1} Ω cm) would be 6280 and 1570 Ω, by Vollebregt et al.[20] (resistivity = 2.2×10^{-2} Ω cm) would be 176 and 44 Ω, by van der Veen et al.[25] (resistivity = 3.0×10^{-2} Ω cm) would be 240 and 60 Ω, and by Jiang et al.[27] (resistivity = 2.1×10^{-2} Ω cm) for a flip-chip densified CNT bundle would be 170 and 42 Ω, respectively; values more than twice that found in this study. However, the resistivity of CNT-based vias reported by Yokoyama et al.[19,51] is better (6.98×10^{-4} Ω cm) than this work which may be because of CMP applied to the vias and higher CNT density (1.6×10^{11} cm^{-2} with seven shells per tube) in their case. CMP is known to disrupt the capped CNT structure and give good electrical contact to many inner CNT shells.[51] A CNT density higher than 10^{12} cm^{-2} has been reported by various groups[21,26,52] using different techniques; some may be applicable for the PTCVD production of densely packed high quality CNTs for future work. The resistivity of our CNT vias is higher than that found with conventional metals. The resistivity of CNT bundles can be improved by optimizing the metal-CNT contacts, applying CMP and increasing the density of carbon nanotubes.

For a density of 10^{10} tubes per cm² and assuming only one conducting shell per tube, the resistance of a single nanotube is calculated to be 250 kΩ and corresponding resistivity to be 12 kΩ μm^{-1}, which is comparable to the CNTs grown at temperatures above 900 °C.[53,54] Although the average number of shells is 9 in our CNTs, the assumption of one conducting shell per tube is in accordance with previous studies[25,51,54–56] and is reasonable since no additional treatment (such as CMP) was given to get access to the inner shells for a direct metal contact. In the case of pure ballistic conduction and perfect metal-CNT contact, each CNT should pose a quantum resistance[57] of 6.45 kΩ in the bundle, resulting in the resistance values of 0.645 and 2.58 Ω for 10 × 10 nd 5 × 5 μm² vias, respectively, which are much smaller than our calculated values of 25 and 100 Ω. The origin of additional high resistance may be because of imperfect metal-CNT contacts, diffusive conduction in the CNTs because of structural defects and oxidation of catalyst, as the sample was exposed to the atmosphere when transferred from sputter deposition system to the PTCVD system.[16,50,58] Assuming diffusive conduction and perfect metal-CNT contact, the resistance of a single CNT (250 kΩ in our case) is given from ref.[57] as $R_{CNT} \approx \frac{h}{4e^2}\frac{l_{CNT}}{l_{mfp}}$, where $h/4e^2$ (6.45 kΩ) is the quantum resistance, l_{CNT} is the length (20 μm in our case) and l_{mfp} is the mean free path of electrons. Using the above equation the mean free path of electrons for as-grown CNTs is estimated to be 515 nm which is two orders of magnitude higher when compared with low temperature (470 °C) grown

CNTs by Chiodarelli et al.,[16] indicating a high structural quality of our tubes.

Finally, the value of R_m after annealing is found to be 251 ± 41 Ω and is worthy of comment. The sheet resistances of M1 (Ti/Cu/TiN) and M2 (Al) are measured separately, using dedicated structures, as 0.16 and 0.18 Ω sq^{-1}, respectively, which subsequently give the resistance of a metal line as 0.6 ± 0.05 Ω; a negligible value as compared with the calculated value of 251 Ω. The increased resistance of R_m is likely be due to the poor metal contact at the joints of the two metal strips due to the step coverage problem as observed in the SEM image analysis of Figure S3a, Supporting Information, and poor metal contact around the edges of the CNT-based vias as observed in SEM image of Figure S2b,Supporting Information. Increased resistance can also be due to the formation of native oxides during the CNT growth process.[58,59] Hofmann et al. studied the CNT growth process on a Ta/Fe structure and observed the oxidation of Ta and reduction of Fe as the temperature exceeds 550 °C, using in situ X-ray photoemission spectroscopy.[58] Similarly, Zhang et al. reported the formation of Al_2O_3 after annealing an Al/Ni bilayer structure in a H_2 gas environment at 800 °C.[59] In view of these reports it is possible that the portions of the Al which are under the CNT growth sites may have been oxidized and so further improvements will be possible with better controlled processing steps.

3. Conclusion

The growth of high quality multiwalled carbon nanotubes on conducting metallic layers at substrate temperatures below 440 °C is demonstrated. The CNT growth profile is observed to vary with respect to the thickness of TiN under-layer which provides an opportunity to fine-tune the various parameters of the CNTs such as diameter, density, number of shells, metallicity and material quality. The highest quality (I_D/I_G = 0.13) and high growth rate (5.6 μm min^{-1}) of carbon nanotubes is achieved using a 100 nm TiN layer. The achieved quality of low temperature (420 °C) grown CNTs on metallic layers is the highest reported thus far and is comparable with arc-discharge produced tubes. Key to the material quality is the ability to control the energy coupled to the catalyst particles. The growth of high quality MWCNTs in via-chain structures is demonstrated under CMOS compatible conditions. At a density of about 10^{10} tubes per cm^2 the electrical resistance values of 25 and 100 Ω for a 10×10 and 5×5 μm^2 via, respectively, are some of the lowest reported to date.

4. Experimental Section

The multilayer structure for the growth of high quality CNTs is shown in Figure 1 where TiN is first sputter deposited on a *n*-Si substrate followed by the deposition of 10 nm Al (as co-catalyst) and 3 nm Fe (as catalyst) layers, respectively. TiN is used because it acts as a thermal barrier layer in PTCVD[60] and a diffusion barrier layer for Cu in interconnect technology. These layers are sequentially deposited without breaking vacuum using JLS-design MPS 500 sputter kit. The thickness of the TiN layer is set as 50, 100, 150, and 200 nm for various samples. Nanotube growth is carried out in a PTCVD system at substrate bulk temperature of 350–440 °C. The method for PTCVD growth of carbon nanomaterials has been reported elsewhere.[22,23,60] Briefly, during PTCVD, energy is delivered directly to the catalyst from the top by optical lamps situated in the head of the reaction chamber, while the sample is placed on a water-cooled platform, as shown in Figure 1b. There are eight lamps (GE lighting model reference 88449-CP77 FEP 230–240 V) arranged in a circular geometry and deliver energy in the reaction chamber through a quartz plate, which acts to isolate the optical head from the chamber. The bulk temperature of the sample is recorded by a pyrometer present at the reverse under side of the substrate whereas the catalyst top surface temperature is recorded by a thermocouple.[22–24] The sample temperature is mainly controlled by the electrical power supplied to the optical lamps, process pressure and flow rate of the gases.[60] Under the current CNT growth conditions, the catalyst top surface temperatures reaches 550–715 °C, while the corresponding bulk temperature of the sample remains between 350–440 °C, as the electrical power supplied to the optical lamps is increased from 30%–50% (100% power = 8 kW). Samples are preheated in flowing H_2 (100 sccm) for 10 min at 2 Torr pressure followed by the CNT growth for 5 min using 10 sccm C_2H_2 as carbon feedstock.

The process flow for the fabrication of CNT-based vias is shown in Figure 8. A layer stack of Ti/Cu/TiN (15/200/50 nm), referred to as "M1," is sputter deposited onto a 150 nm SiO_2 coated *n*-Si substrate and patterned lithographically using lift-off process (Figure 8 – step 1). Ti/Cu/TiN layer stack is commonly used in integrated circuit interconnects, where Ti and TiN act as diffusion barrier layers for Cu. Samples are air transferred to JLS-design DP 80 kit where a plasma enhanced CVD of 300 nm SiO_2 film is carried-out using silane and N_2O_2. The SiO_2 film is patterned lithographically and etched down to M1 to define via holes (Figure 8 – step 2). A 10 nm Al film as a co-catalyst and a 3 nm Fe film as a catalyst for CNT growth are sputter deposited in the etched holes and samples are air transferred to the PTCVD system where CNT growth is carried out at substrate bulk temperature of 400 °C (Figure 8 – step 3) under the conditions described earlier. Finally, a 300 nm Al film (M2) is sputter deposited, patterned and etched (Figure 8 – step 4) as top metal lines. Samples are then annealed at 450 °C in a He environment for 30 min and electrical measurements were performed before, and after the annealing. The as-grown CNTs are characterized using a FEI Quanta 200 scanning electron microscope, Raman spectroscopy (Renishaw Systems 2000) using 514 nm laser wavelength, a Philips CM200 transmission electron microscope (TEM) and a Keithley 4200 analyzer for electrical measurements.

Supporting Information

Supporting Information is available from the Wiley Online Library or from the author.

Acknowledgements

The authors acknowledge funding from EPSRC (UK). The authors confirm that data underlying the findings are available without restriction. Details of the data and how to request access are available from the University of Surrey publications repository http://epubs.surrey.ac.uk/807660/.

Received: March 26, 2015
Revised: May 11, 2015
Published online: June 8, 2015

[1] M. Endo, M. S. Strano, P. M. Ajayan, *Carbon Nanotubes* **2008**, *111*, 13.
[2] J. Robertson, G. Zhong, C. S. Esconjauregui, B. C. Bayer, C. Zhang, M. Fouquet, S. Hofmann, *Jpn. J. Appl. Phys.* **2012**, *51*, 01AH01.

[3] Y. Awano, S. Sato, M. Nihei, T. Sakai, Y. Ohno, T. Mizutani, *Proc. IEEE* **2010**, *98*, 2015.
[4] T. Wang, K. Jeppson, N. Olofsson, E. E. B. Campbell, J. Liu, *Nanotechnology* **2009**, *20*, 485203.
[5] A. P. Graham, G. S. Duesberg, R. V. Seidel, M. Liebau, E. Unger, W. Pamler, F. Kreupl, W. Hoenlein, *Small* **2005**, *1*, 382.
[6] P. Avouris, Z. Chen, V. Perebeinos, *Nat. Nanotechnol.* **2007**, *2*, 605.
[7] S. Vollebregt, R. Ishihara, F. D. Tichelaar, Y. Hou, C. I. M. Beenakker, *Carbon* **2012**, *50*, 3542.
[8] G. Zhong, T. Iwasaki, J. Robertson, H. Kawarada, *J. Phys. Chem. B* **2007**, *111*, 1907.
[9] K. Hata, D. N. Futaba, K. Mizuno, T. Namai, M. Yumura, S. Iijima, *Science* **2004**, *306*, 1362.
[10] M. Cantoro, S. Hofmann, S. Pisana, V. Scardaci, A. Parvez, C. Ducati, A. C. Ferrari, A. M. Blackburn, K. Y. Wang, J. Robertson, *Nano Lett.* **2006**, *6*, 1107.
[11] M. S. Shamsudin, N. A. Asli, S. Abdullah, S. Y. S. Yahya, M. Rusop, *Adv. Condens. Matter Phys.* **2012**, *7*, 420619.
[12] Y. T. Lee, J. Park, Y. S. Choi, H. Ryu, H. J. Lee, *J. Phys. Chem. B* **2002**, *106*, 7614.
[13] K. E. Kim, K. J. Kim, W. S. Jung, S. Y. Bae, J. Park, J. Choi, J. Choo, *Chem. Phys. Lett.* **2005**, *401*, 459.
[14] E. R. Meshot, D. L. Plata, S. Tawfick, Y. Zhang, E. A. Verploegen, A. J. Hart, *ACS Nano* **2009**, *3*, 2477.
[15] Y. T. Lee, N. S. Kim, J. Park, J. B. Han, Y. S. Choi, H. Ryu, H. J. Lee, *Chem. Phys. Lett.* **2003**, *372*, 853.
[16] N. Chiodarelli, S. Masahito, Y. Kashiwagi, Y. Li, K. Arstila, O. Richard, D. J. Cott, M. Heyns, S. De Gendt, G. Groeseneken, P. M. Vereecken, *Nanotechnology* **2011**, *22*, 085302.
[17] J. Dijon, A. Fournier, P. D. Szkutnik, H. Okuno, C. Jayet, M. Fayolle, *Diamond Relat. Mater.* **2010**, *19*, 382.
[18] J. Robertson, G. Zhong, S. Hofmann, B. C. Bayer, C. S. Esconjauregui, H. Telg, C. Thomsen, *Diamond Relat. Mater.* **2009**, *18*, 957.
[19] D. Yokoyama, T. Iwasaki, K. Ishimaru, S. Sato, T. Hyakushima, M. Nihei, Y. Awano, H. Kawarada, *Jpn. J. Appl. Phys.* **2008**, *47*, 1985.
[20] S. Vollebregt, F. D. Tichelaar, H. Schellevis, C. I. M. Beenakker, R. Ishihara, *Carbon* **2014**, *71*, 249.
[21] N. Na, D. Y. Kim, Y. G. So, Y. Ikuhara, S. Noda, *Carbon* **2015**, *81*, 773.
[22] M. Ahmad, J. V. Anguita, V. Stolojan, J. D. Carey, S. R. P. Silva, *ACS Appl. Mater. Interfaces* **2013**, *5*, 3861.
[23] J. V. Anguita, D. C. Cox, M. Ahmad, Y. Y. Tan, J. Allam, S. R. P. Silva, *Adv. Funct. Mater.* **2013**, 5502.
[24] J.-S. Chen, V. Stolojan, S. R. P. Silva, *Carbon* **2015**, *84*, 409.
[25] M. H. van der Veen, B. Vereecke, C. Huyghebaert, D. J. Cott, M. Sugiura, Y. Kashiwagi, L. Teugels, R. Caluwaerts, N. Chiodarelli, P. M. Vereecken, G. P. Beyer, M. M. Heyns, S. De Gendt, Z. Tokei, *Microelectron. Eng.* **2013**, *106*, 106.
[26] J. Dijon, H. Okuno, M. Fayolle, T. Vo, J. Pontcharra, D. Acquaviva, D. Bouvet, A. M. Ionescu, C. S. Esconjauregui, B. Capraro, E. Quesnel, J. Robertson, in IEEE 2010 Int. Electron Devices Meet., Tech. Dig., IEEE, San Francisco, CA **2010**.
[27] D. Jiang, T. Wang, S. Chen, L. Ye, J. Liu, *Microelectron. Eng.* **2013**, *103*, 177.
[28] N. Chiodarelli, Y. Li, D. J. Cott, S. Mertens, N. Peys, M. Heyns, S. De Gendt, G. Groeseneken, P. M. Vereecken, *Microelectron. Eng.* **2011**, *88*, 837.
[29] S. Esconjauregui, R. Xie, M. Fouquet, R. Cartwright, D. Hardeman, J. Yang, J. Robertson, *J. Appl. Phys.* **2013**, *113*, 144309.
[30] R. Saito, A. Gruneis, G. G. Samsonidze, V. W. Brar, G. Dresselhaus, M. S. Dresselhaus, A. Jorio, L. G. Cancado, C. Fantini, M. A. Pimenta, A. G. Souza, *New J. Phys.* **2003**, *5*, 157.
[31] F. Tuinstra, J. L. Koenig, *J. Chem. Phys.* **1970**, *53*, 1126.
[32] Y. Wang, D. C. Alsmeyer, R. L. McCreery, *Chem. Mater.* **1990**, *2*, 557.
[33] J. Campos-Delgado, Y. A. Kim, T. Hayashi, A. Morelos-Gomez, M. Hofmann, H. Muramatsu, M. Endo, H. Terrones, R. D. Shull, M. S. Dresselhaus, M. Terrones, *Chem. Phys. Lett.* **2009**, *469*, 177.
[34] K. Behler, S. Osswald, H. Ye, S. Dimovski, Y. Gogotsi, *J. Nanoparticle Res.* **2006**, *8*, 615.
[35] J. Ziebro, I. Lukasiewicz, E. Borowiak-Palen, B. Michalkiewicz, *Nanotechnology* **2010**, *21*, 145308.
[36] H. X. Qiu, Z. J. Shi, L. H. Guan, L. P. You, M. Gao, S. L. Zhang, J. S. Qiu, Z. N. Gu, *Carbon* **2006**, *44*, 516.
[37] M. Chhowalla, K. B. K. Teo, C. Ducati, N. L. Rupesinghe, G. A. J. Amaratunga, A. C. Ferrari, D. Roy, J. Robertson, W. I. Milne, *J. Appl. Phys.* **2001**, *90*, 5308.
[38] S. P. Patole, P. S. Alegaonkar, H.-C. Lee, J.-B. Yoo, *Carbon* **2008**, *46*, 1987.
[39] N. G. Shang, Y. Y. Tan, V. Stolojan, P. Papakonstantinou, S. R. P. Silva, *Nanotechnology* **2010**, *21*, 505604.
[40] Y. Tison, C. E. Giusca, V. Stolojan, Y. Hayashi, S. R. P. Silva, *Adv. Mater.* **2008**, *20*, 189.
[41] L. T. Qu, F. Du, L. M. Dai, *Nano Lett.* **2008**, *8*, 2682.
[42] http://www.filmetrics.com/reflectance-calculator (accessed: January **2014**).
[43] T. Wang, D. Jiang, S. Chen, K. Jeppson, L. Ye, J. Liu, *Mater. Lett.* **2012**, *78*, 184.
[44] T. T. Vo, C. Poulain, J. Dijon, A. Fournier, N. Chevalier, D. Mariolle, *J. Appl. Phys.* **2012**, *112*, 044901.
[45] H. Li, N. Srivastava, J. F. Mao, W. Y. Yin, K. Banerjee, *IEEE Trans. Electron Devices* **2011**, *58*, 2689.
[46] M. K. Majumder, N. D. Pandya, B. K. Kaushik, S. K. Manhas, *IEEE Electron Device Lett.* **2012**, *33*, 1180.
[47] M. Sahoo, P. Ghosal, H. Rahaman, *J. Comput. Electron.* **2014**, *13*, 673.
[48] G. S. Duesberg, A. P. Graham, M. Liebau, R. Seidel, E. Unger, F. Kreupl, W. Hoenlein, *Nano Lett.* **2003**, *3*, 257.
[49] H. J. Li, W. G. Lu, J. J. Li, X. D. Bai, C. Z. Gu, *Phys. Rev. Lett.* **2005**, *95*, 086601.
[50] M. Katagiri, M. Wada, B. Ito, Y. Yamazaki, M. Suzuki, M. Kitamura, T. Saito, A. Isobayashi, A. Sakata, N. Sakuma, A. Kajita, T. Sakai, *Jpn. J. Appl. Phys.* **2012**, *51*, 05ED02.
[51] D. Yokoyama, T. Iwasaki, T. Yoshida, H. Kawarada, S. Sato, T. Hyakushima, M. Nihei, Y. Awano, *Appl. Phys. Lett.* **2007**, *91*, 263101.
[52] S. Esconjauregui, M. Fouquet, B. C. Bayer, C. Ducati, R. Smajda, S. Hofmann, J. Robertson, *ACS Nano* **2010**, *4*, 7431.
[53] S. D. Li, Z. Yu, C. Rutherglen, P. J. Burke, *Nano Lett.* **2004**, *4*, 2003.
[54] B. Bourlon, C. Miko, L. Forro, D. C. Glattli, A. Bachtold, *Phys. Rev. Lett.* **2004**, *93*, 176806.
[55] P. Delaney, M. Di Ventra, S. T. Pantelides, *Appl. Phys. Lett.* **1999**, *75*, 3787.
[56] S. Frank, P. Poncharal, Z. L. Wang, W. A. de Heer, *Science* **1998**, *280*, 1744.
[57] C. Rutherglen, P. Burke, *Small* **2009**, *5*, 884.
[58] B. C. Bayer, M. Fouquet, R. Blume, C. T. Wirth, R. S. Weatherup, K. Ogata, A. Knop-Gericke, R. Schloegl, S. Hofrnann, J. Robertson, *J. Phys. Chem. C* **2012**, *116*, 1107.
[59] R. Y. Zhang, L. Amlani, J. Baker, J. Tresek, R. K. Tsui, *Nano Lett.* **2003**, *3*, 731.
[60] G. Y. Chen, B. Jensen, V. Stolojan, S. R. P. Silva, *Carbon* **2011**, *49*, 280.